Materials Today Communications 25 (2020) 101418

Contents lists available at ScienceDirect

Materials Today Communications

journal homepage: www.elsevier.com/locate/mtcomm

Bisbenzylidene cyclopentanone and cyclohexanone-functionalized polybenzoxazine nanocomposites: Synthesis, characterization, and use for corrosion protection on mild steel

Mohamed Gamal Mohamed[a,b,*], Shiao Wei Kuo[b], Abdulsalam Mahdy[a,c], Ibrahim M. Ghayd[d], Kamal. I. Aly[a,**]

[a] Polymer Research Laboratory, Chemistry Department, Faculty of Science, Assiut University, Assiut, 71516, Egypt
[b] Department of Materials and Optoelectronic Science, Center of Crystal Research, National Sun Yat-Sen University, Kaohsiung, Taiwan
[c] Chemistry Department, Faculty of Education & Science - Rada'a Al-Baydha University, Yemen
[d] Central Metallurgical Research and Development Institute, P. O. Box: Helwan, Cairo, Egypt

ARTICLE INFO

Keywords:
Benzoxazine resin
Polybenzoxazine
Thermal curing polymerization
Nanocomposites
Corrosion behavior

ABSTRACT

In this study, we synthesized and investigated bisbenzylidene cyclopentanone and cyclohexanone-functionalized polybenzoxazine nanocomposites as anti-corrosion coatings. The chemical structures of CP-BZ and CH-BZ were confirmed using Fourier transform infrared (FTIR) spectroscopy and ^{1}H and ^{13}C nuclear magnetic resonance spectroscopy. Differential scanning calorimetry (DSC) revealed that the thermal polymerization temperature of the uncured CH-BZ (198 °C) was significantly lower than that of the monomer 3-phenyl-3,4-dihydro-2*H*-benzoxazine (263 °C). We used DSC and FTIR spectroscopy to study the curing behavior of these monomers. The degradation temperature of poly(CH-BZ) (326 °C) was higher than that poly(CP-BZ) (249 °C), based on thermogravimetric analysis. We used solution dispersion and thermal ring-opening polymerization to prepare a new class of bisbenzylidene-based polybenzoxazine (PBZ; CP-BZ or CH-BZ) composites with epoxidized soybean oil (E-SBO; 10 or 20 wt%) and E-SBO/bentonite (nanoclay; 3 or 5 wt%) for use as corrosion-protection coatings for mild steel (MS). We employed salt-spray and electrochemical measurements to investigate the influence of the epoxy and nanoclay contents, respectively, on the corrosion-resistance of these coatings. A 20 wt% epoxy content in the PBZ/E-SBO coatings provided corrosion-resistance superior to those of pure PBZs. Furthermore, the addition of 20 wt% E-SBO and 3 wt% of nanoclay decreased the corrosion rate by one order of magnitude (2.653×10^{-3} mm year^{-1}) when compared with that of pure poly(CH-BZ) (1.292×10^{-2} mm year–1) and two orders of magnitude when compared with blank(MS) (1.094×10^{-1} mm year^{-1}) with protection efficiency (98.16 %), revealing markedly increased barrier properties of the composite coatings towards corrosive species. Thus, these materials function as excellent corrosion-resistance coatings for MS.

1. Introduction

Polybenzoxazines (PBZs) are thermosetting polymers that can be prepared through ring-opining polymerization (ROP) of benzoxazine (BZ) monomers in the absence of any catalysts, with no byproducts released during their thermal curing polymerization [1–8]. The attractive properties PBZs include high thermal stabilities, low dielectric constants, chemical resistance, high glass transition temperatures (T_g), low surface energies, low water absorption, zero-near shrinkage upon curing, and good flame-retardancy [9–15]. Most of these properties are related to PBZs having a high density of inter- and intramolecular hydrogen bonds between their phenolic groups and nitrogen-containing Mannich-type bridges [16–24]. Although PBZ resins have been applied in various applications (e.g., in the electronics industry and as high-temperature coatings and flame-retardant coatings), their use as coatings generally suffers from the brittleness of their films and the need for high curing temperatures. To overcome these obstacles, additional functional groups (e.g., cyano, amine, allyl, hydroxyl) can be incorporated into the BZ resins by reacting a multifunctional amine with a mono-phenol or a multifunctional phenolic resin with a monoamine [25–31]. Recently, polymers containing bisbenzylidene moieties as photo- and thermo-sensitive segments in their side or main chains have

* Corresponding author at: Polymer Research Laboratory, Chemistry Department, Faculty of Science, Assiut University, Assiut, 71516, Egypt.
** Corresponding author.
E-mail addresses: mgamal.eldin12@yahoo.com (M.G. Mohamed), kamalaly@aun.edu.eg (K.I. Aly).

https://doi.org/10.1016/j.mtcomm.2020.101418
Received 19 April 2020; Received in revised form 29 June 2020; Accepted 30 June 2020
Available online 03 July 2020

become attractive materials in academia and industry because of their potential applications in photo recorders, photocurable coatings, energy exchange materials, and printing plates [32–39]. The light- and heat-activated polymerizations of olefinic (e.g., coumarin and chalcone) BZ monomers have been studied [7,8,32–39]. Furthermore, BZs monomers have been used as blends with epoxy resins to enhance the adhesion of polymers and increase their corrosion-resistance [40–42]. Rimdusit et al. [43] investigated the effects of epoxy resin on various arylamine-based BZ resins [aniline, m-toluidine, 3,5-xylidine]; they found that the mechanical properties of prepared blend were enhanced upon increasing the amount of the epoxy. Organic corrosion-protection coatings applied on metallic surfaces form a barrier between the metal surface and its environment, preventing or delaying the transportation of corrosive species toward the metal and, thereby, retarding the creation of rust at the metal surface [40–42]. Coating mild steel (MS) with PBZ resins can decrease the corrosion rate (CR) because the PBZs possess hydrophobic properties, nitrogen atoms, conjugated π-electrons, and large molecular sizes [42]. For example, MS coated with a guaiacol-based poly(BZ-urethane) through salt-spraying displayed enhanced corrosion-resistance upon increasing the urethane content in the polymer backbone [44]. In recent years, the co-curing of BZ monomers with phenolic and epoxy resins has become the most effective method for enhancing the adhesion properties, hardness, thermal properties, mechanical properties, and corrosion-resistance of PBZ films [40–42]. Furthermore, the incorporation of nanoclays can improve the barrier properties of polymeric coatings by decreasing their permeability and increasing the lengths of the diffusion pathways for O_2 and water [45]. In 2020, our group observed that coating MS with epoxidized soybean oil (E-SBO) and poly(azine-BZ–CH_3)/nanoclay led to more efficient corrosion protection (99.63 %) [46]. In 2020, Alagar et al. successfully prepared bio-based polybenzoxazine composite by using cardanol, eugenol and bio-silica as reinforcement. They found that these coating composites on MS showed excellent resistance to corrosion [47]. Andronescu and his group synthesized different types from BZ derivatives by using phenolated methyl oleate as the phenol source with aniline,1,6-diaminohexane, or 4,4'-diaminodiphenylmethane, respectively. They revealed that Zn-Mg-Al-steel sheets coated with polybenzoxazine coatings displayed increased OCP value and breakthrough potential [48]. Mhaske and his workers successfully prepared GPTMS (glycidoxypropyltrimethoxysilane)-modified Bnz coatings and these materials improved the barrier protection to corrosive species because of its highly crosslinked structure [49]. Also, Andronescu et al. reported that coating Zn–Mg–Al alloy with benzoxazine derivatives, which were synthesized using phenolated high oleic sunflower oil and 1,6-diaminohexan showed increased OCP value [50]. In this present paper, we report the curing behaviour of cyclopentanone (CP)-BZ and cyclohexanone (CH)-BZ, subsequent characterization of PBZ/E-SBO/nanoclay materials and their application as anti-corrosion coatings. First, we prepared bis(benzylidene)CP-2OH and bis(benzylidene)CH-2OH through aldol condensations of 4-hydroxybenzaldehyde with CP and CH, respectively, under acidic conditions. Then, we synthesized the monomers CP-BZ and CH-BZ through Mannich condensations of bis(benzylidene)CP-2OH and bis(benzylidene)CH-2OH, respectively, with *p*-toluidine and paraformaldehyde [$(CH_2O)_n$] in 1,4-dioxane. We characterized these monomers using ^1H and ^{13}C nuclear magnetic resonance (NMR) spectroscopy and Fourier transform infrared (FTIR) spectroscopy and studied the ROPs of their oxazine rings using differential scanning calorimetry (DSC) and in situ FTIR spectroscopy. Thermogravimetric analysis (TGA) revealed the thermal stabilities of the resulting polymers. Finally, we used salt-spray and electrochemical (polarization measurement) techniques to examine the corrosion resistance of MS coated with pure PBZ with epoxy resin [poly(CP-BZ)/E-SBO (10 and 20 wt%), poly(CH-BZ)/E-SBO (10 and 20 wt %)] and also PBZ with epoxy and composites [poly(CP-BZ)/E-SBO (20 wt%)/nanoclay (3 and 5 wt%), and poly(CH-BZ)/E-SBO (20 wt%)/nanoclay (3 and 5 wt%)] in 3.5 wt % NaCl aqueous solutions.

2. Experimental section

2.1. Materials

CP, CH, 4-hydroxybenzaldehyde, *p*-toluidine, $(CH_2O)_n$, sodium hydroxide (NaOH), HCl (37 %), anhydrous magnesium sulfate ($MgSO_4$), chloroform ($CHCl_3$), absolute ethanol (EtOH), 1,4-dioxane, ethyl acetate (EtOAc), glacial acetic acid (AcOH), and hydrogen peroxide (H_2O_2) were obtained from Acros. Sodium bentonite (nanoclay) and hexadecyl trimethyl ammonium bromide (HTAB) were purchased from Aldrich (Hamburg, Germany). Bis(benzylidene)CP-2OH and Bis(benzylidene)CP-2OH were synthesized according to the reported methods [Figs. S1 and S2] [51,52].

2.2. (2E,5E)-2,5-Bis((3,4-dihydro-3-p-tolyl-2H-benzo[e][1,3]oxazine-6-yl)methylene)cyclopentanone (CP-BZ)

A solution of $(CH_2O)_n$ (0.800 g, 27.0 mmol) and *p*-toluidine (1.60 g, 15.0 mol) in 1,4-dioxane (30 mL) was heated under reflux in a 100-mL round-bottom flask with stirring at 70 °C for 30 min. Bis(benzylidene)CP-2OH (2.00 g, 7.00 mol) was added and then the temperature was gradually raised to 110 °C and stirring continued for 24 h. The solvent was evaporated using a rotary evaporator. The yellowish residue was dissolved in EtOAc and washed three times with 1 N NaOH and twice with distilled water. The organic layer was dried ($MgSO_4$), filtered, and concentrated (rotary evaporator) to afford a wine-red product (85 %). ^1H NMR (400 MHz, DMSO-d_6, δ, ppm): 6.8–7.6 (m, 14H, ArH), 5.30 (s, 4H, OCH_2N), 4.50 (s, 4H, $ArCH_2N$). ^{13}C NMR (400 MHz, $CDCL_3$, δ, ppm): 191.31 (C═O), 80.62 (NCH_2O), 49.98 ($ArCH_2N$), 26.72 (CH_3), 25.26 ($2CH_2$ of CP). FTIR (KBr, cm^{-1}): 2917, 2857 (symmetric and asymmetric stretching of CP moiety), 1668 (C═O), 1580 (CC═), 1467 (stretching of trisubstituted benzene ring), 1232 (asymmetric C−OC− stretching), 940 (out-of-plane C−H bending). UV–vis λ_{max} ($CHCl_3$): 380 nm (-C = C-) [Fig. S3(a)].

2.3. (2E,6E)-2,6-Bis((3,4-dihydro-3-p-tolyl-2H-benzol[e][1,3]oxazin-6-yl)methylene)cyclohexanone (CH-BZ)

A solution of $(CH_2O)_n$ (0.800 g, 27.0 mmol) and *p*-toluidine (1.60 g, 15.0 mmol) in 1,4-dioxane (50 mL) was heated under reflux in a 100-mL round-bottom flask with stirring at 70 °C for 30 min. Bis(benzylidene)CH-2OH) (2.00 g, 7.00 mmol) was added and then the temperature was gradually raised to 110 °C and stirring continued for 24 h. The solvent was evaporated using a rotary evaporator. The residue was dissolved in EtOAc and washed three times with 1 N NaOH and twice with distilled water. The organic phase was dried ($MgSO_4$), filtered, and concentrated (rotary evaporator) to afford a red solid (90 %). ^1H NMR (400 MHz, DMSO-d_6, δ, ppm): 6.8–7.6 (m, 14H, ArH), 5.40 (s, 4H, OCH_2N), 4.60 (s, 4H, $ArCH_2N$), 2.3 (s, CH_3). ^{13}C NMR (400 MHz, $CDCL_3$, δ, ppm): 190.32 (C═O), 80.38 (OCH_2N), 50.79 ($ArCH_2N$), 29.69 (CH_2 of CH), 28.50 (CH_2 of CH), 20.48 (CH_3). FTIR (KBr, cm^{-1}): 2917, 2857 (symmetric and asymmetric stretching of CH moiety), 1654 (C═O), 1594 (CC═), 1497 (stretching of trisubstituted benzene ring), 1235 (asymmetric C−OC− stretching), 935 (out-of-plane C−H bending). UV–vis λ_{max} ($CHCl_3$): 365 nm (-C = C-) [Fig. S3(b)].

2.4. Poly(CP-BZ) and poly(CH-BZ)

Poly(CP-BZ) and poly(CH-BZ) were obtained through thermal ROP of the monomers CP-BZ and CH-BZ, respectively, in the absence of an initiator or catalyst (Scheme 2). The curing process was performed with stepwise heating in an air-circulating oven at 110, 150, 180, 210, and 240 °C for 2 h at each temperature and then the samples were cooled slowly to room temperature. The resulting polymers had a dark brown color.

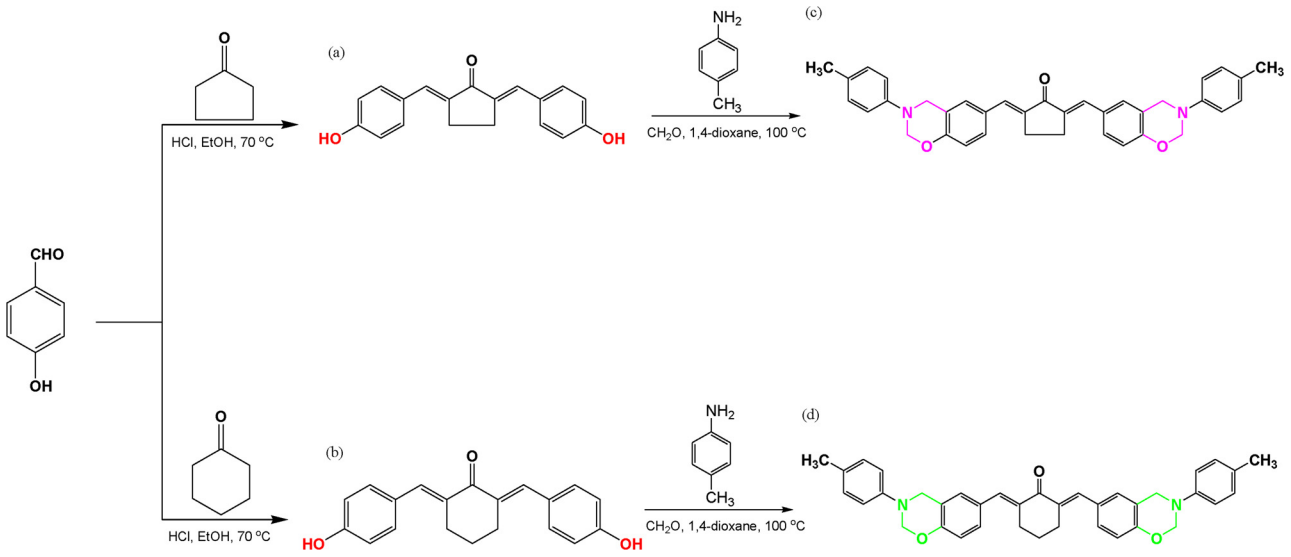

Scheme 1. Synthesis of (a) bis(benzylidene)CP-2OH, (b) bis(benzylidene)CH-2OH, (c) CP-BZ, and (d) CH-BZ.

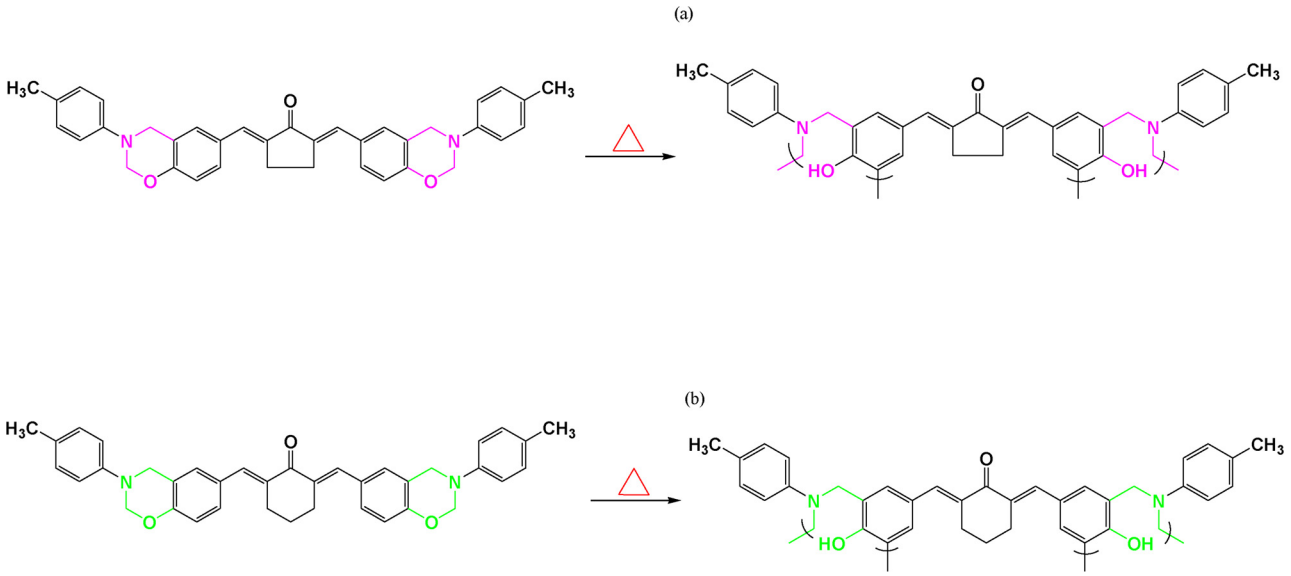

Scheme 2. ROPs of CP-BZ and CH-BZ to afford poly(CP-BZ) and poly(CH-BZ), respectively.

2.5. E-SBO [Scheme S1]

A mixture of soybean oil (100.0 g) in toluene (50 mL), AcOH (15.00 g), and Amberlite (25.00 g) in a 500-mL three-neck flask equipped with a thermometer was stirred magnetically at 60 °C for 5 h. The required amount of H_2O_2 (30 %) was added slowly to the mixture using a titration tube. The reaction time was counted from this point onward. After completion of the reaction, the mixture was cooled to room temperature, placed in a separatory funnel, and washed several times with distilled water (cold–hot–cold) to remove any excess AcOH and H_2O_2. The organic phase was dried (Na_2SO_4) and placed in an oven overnight at 60 °C. FTIR (KBr, cm^{-1}): 2857 and 2928 (CH_2 group), 1744 (C═O stretching), 825 and 845 (epoxy group). ^1H NMR (500 MHz, $CDCl_3$, δ, ppm, Fig. S4): 0.82 (t, 3H, CH_3), 1.5 (br, 2H, CH_2, β to epoxide ring), 1.7 (CH_2 between two epoxy groups), 2.06–2.08 (CH_2 adjacent to double bond), 2.21–2.24 (CH_2 between epoxy ring and double bond), 2.95–3.01 (CH of epoxide ring), 4.04–5.1 (CH_2 of glyceride structure), 5.32–5.42 (2CH, unreacted ethylene bond).

2.6. PBZ/E-SBO coatings

MS surfaces were degreased with acetone and dried. The monomers CP-BZ and CH-BZ and E-SBO were dissolved separately in $CHCl_3$ at a concentration of 100 g L^{-1}. The monomers CP-BZ and CH-BZ were mixed separately with E-SBO (10 or 20 wt% epoxy content), at a molar ratio of approximately 1:1, or without. The mixtures were cast on the MS panels such that the same thickness was achieved for each coated sample. After drying in air for 24 h, the coated panels were cured at 210 °C for 2 h.

2.7. PBZ/E-SBO/nanoclay composite coatings

Poly(CP-BZ)/E-SBO (20 wt% epoxy content)/nanoclay (3 and 5 wt %) and poly(CH-BZ)/E-SBO (20 wt% epoxy content)/nanoclay (3 and 5 wt%) composite coatings were prepared through solution-dispersion. For example, the poly(CP-BZ)/E-SBO/nanoclay (3 wt%) composite coating was prepared as follows: Modified nanoclay [prepared through cation-exchange of sodium bentonite and hexadecyl trimethyl ammonium bromide (HTAB) according to a reported procedure [45]; 0.030 g]

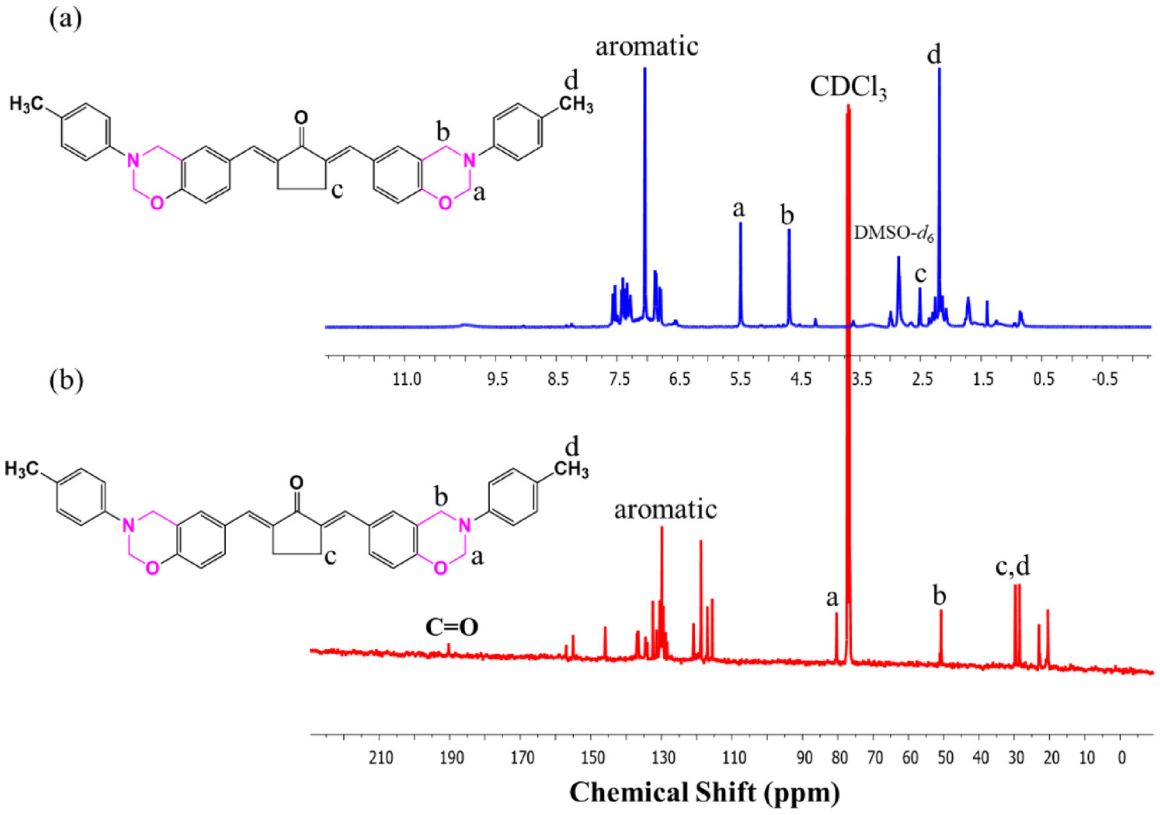

Fig. 1. (a) ^{1}H and (b) ^{13}C NMR spectra of CP-BZ in DMSO-d_6 and $CDCl_3$.

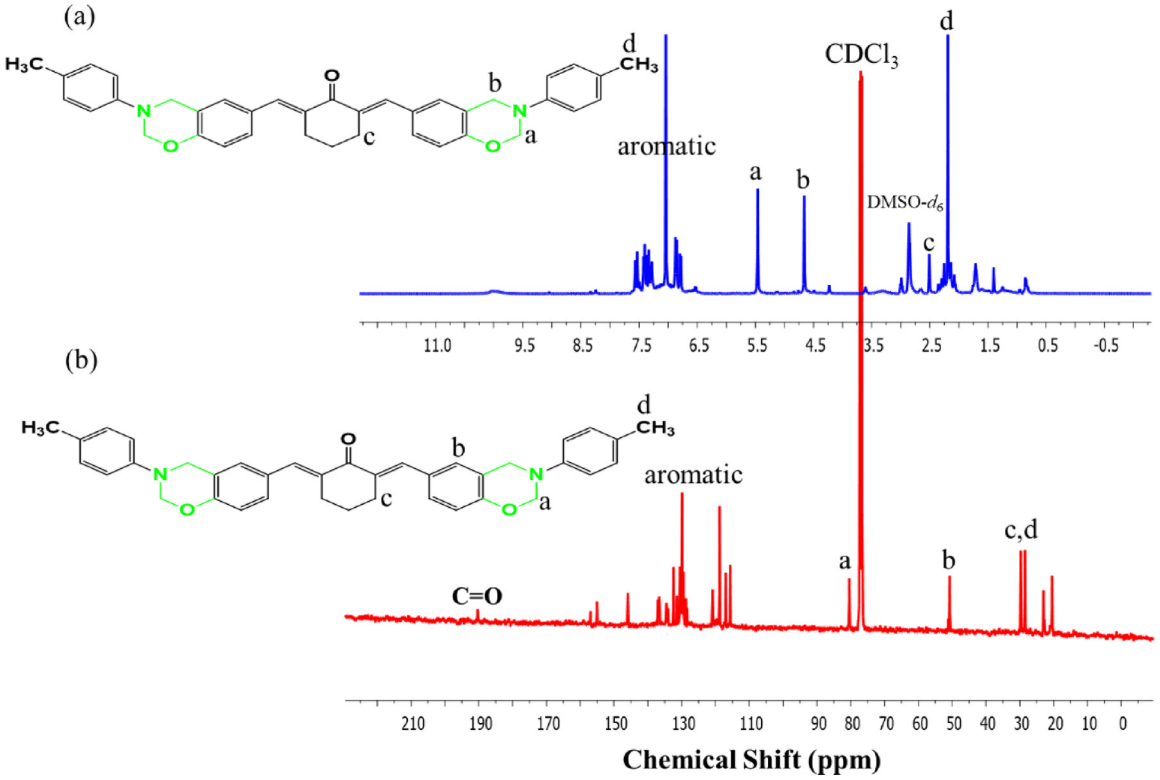

Fig. 2. (a) ^{1}H and (b) ^{13}C NMR spectra of CH-BZ in DMSO-d_6 and $CDCl_3$.

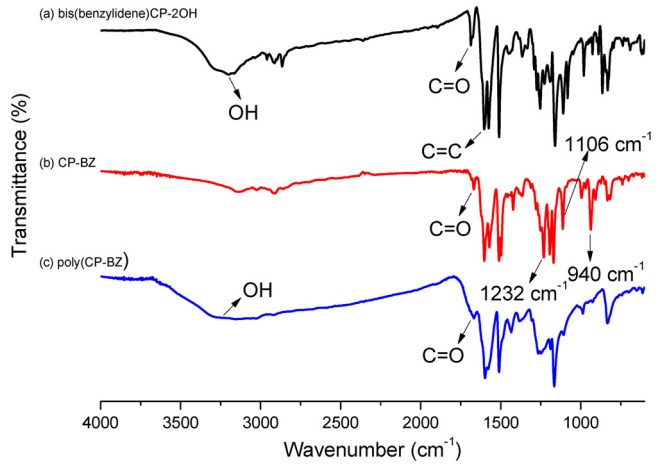

Fig. 3. FTIR spectra of (a) bis(benzylidene)CP-2OH, (b) CP-BZ, and (c) poly(CP-BZ).

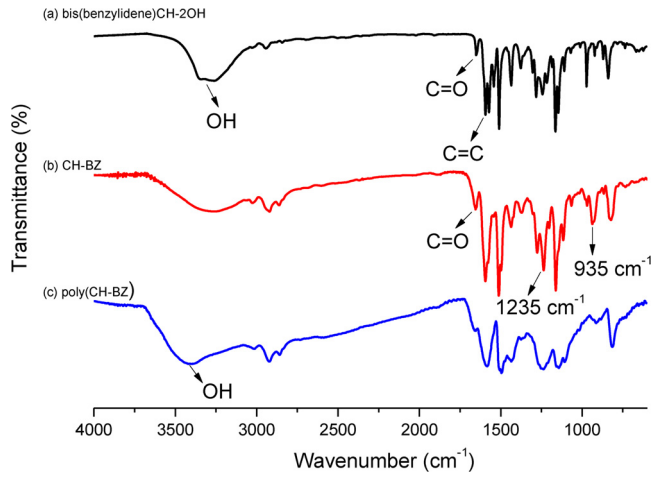

Fig. 4. FTIR spectra of (a) bis(benzylidene)CH-2OH, (b) CH-BZ, and (c) poly (CH-BZ).

was added to a mixture of CP-BZ (0.77 g) and E-SBO epoxy resin (0.20 g) in $CHCl_3$ at 100 g L^{-1}. The mixture was stirred at 80 °C for 5 h and then cast (thickness: 5 μm) onto an MS surface (20 mm × 20 mm) that had been degreased with acetone and distilled water and scrubbed with sandpaper. After drying in air for 24 h, the coated panels were cured at 210 °C for 2 h. The obtained poly(CP-BZ)/E-SBO/nanoclay (3 and 5 wt %) and poly(CH-BZ)/E-SBO/nanoclay (3 and 5 wt%) coating composites were colored brown, as revealed in Fig. S6(e, f, k, l).

2.8. Characterization

FTIR spectra were recorded using a Bruker Tensor 27 FTIR spectrophotometer and the conventional KBr disk method; 32 scans were collected at a spectral resolution of 4 cm^{-1}. The films used in this study were sufficiently thin to obey the Beer–Lambert law. UV absorption spectra were measured between 320 and 420 nm on a Herolab UV-6 S/L LW. Transmission electron microscopy (TEM) images were obtained using a JEOL JEM-2010 instrument operated at 200 kV. The surface morphologies of the MS samples in the presence and absence of polymer coatings (after polarization measurements) were investigated using scanning electron microscopy (SEM; JEOL JSM-7610 F). The dynamic curing behavior of all of the BZ samples (5–7 mg) was determined in a DSC sample cell using a TA Q-20 DSC apparatus, with heating from 30 to 350 °C at 20 °C min^{-1} under an N_2 atmosphere (50 mL min^{-1}). The thermal stabilities of all the BZ samples (5–7 mg) were

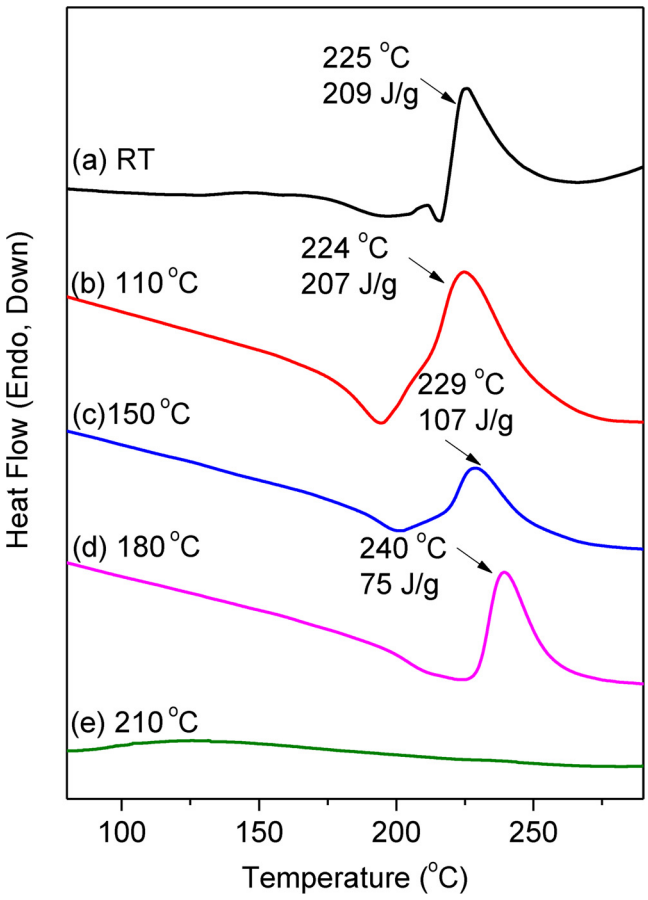

Fig. 5. DSC thermograms of CP-BZ before and after thermal treatment at various temperatures.

measured using a TA Q-50 TGA apparatus, with heating from 30 to 800 °C at 20 °C min^{-1} under an N_2 atmosphere (60 mL min^{-1}).

2.9. Salt-spray technique

The corrosion-resistance of the MS coated with pure poly(CP-BZ), pure poly(CH-BZ), poly(CP-BZ)/E-SBO (10 wt%), poly(CP-BZ)/E-SBO (20 wt%), poly(CH-BZ)/E-SBO (10 wt%), and poly(CH-BZ)/E-SBO (20 wt%) was investigated through the salt-spray technique using a SF/450 salt-spray cabinet (CW Specialist Equipment, England). A work crosscut was made in the middle of each MS panel using a cutter, to permit penetration of the salt solution into the panel and, thereby, examine the adherence of the coating over the painted area [53]. The coated panels were exposed to 5 wt% aqueous NaCl for 500 h at 35 °C according to ASTM B117. The coated panels were examined for blistering, scribe failure, and the degree of rusting according to ASTM D714-94, D1654-92, and D610-95, respectively.

2.10. Electrochemical technique

The corrosion-resistance of MS coated with pure PBZ and PBZ/E-SBO and PBZ/E-SBO/nanoclay composites was investigated through potentiodynamic polarization. Tests were performed using a computerized potentiostat (Autolab PGSTAT 30) in 3.5 % NaCl at room temperature. Prior to measurement, the samples were immersed in the testing solution for 30 min to determine the steady state potential, defined as the free corrosion potential (E_{corr}). The potential was then scanned from –0.3 to +1 V against E_{corr} (scan rate: 0.002 V s^{-1}) for polarization current experiments. The Tafel extrapolation technique was used to measure the corrosion potential (E_{corr}) and corrosion

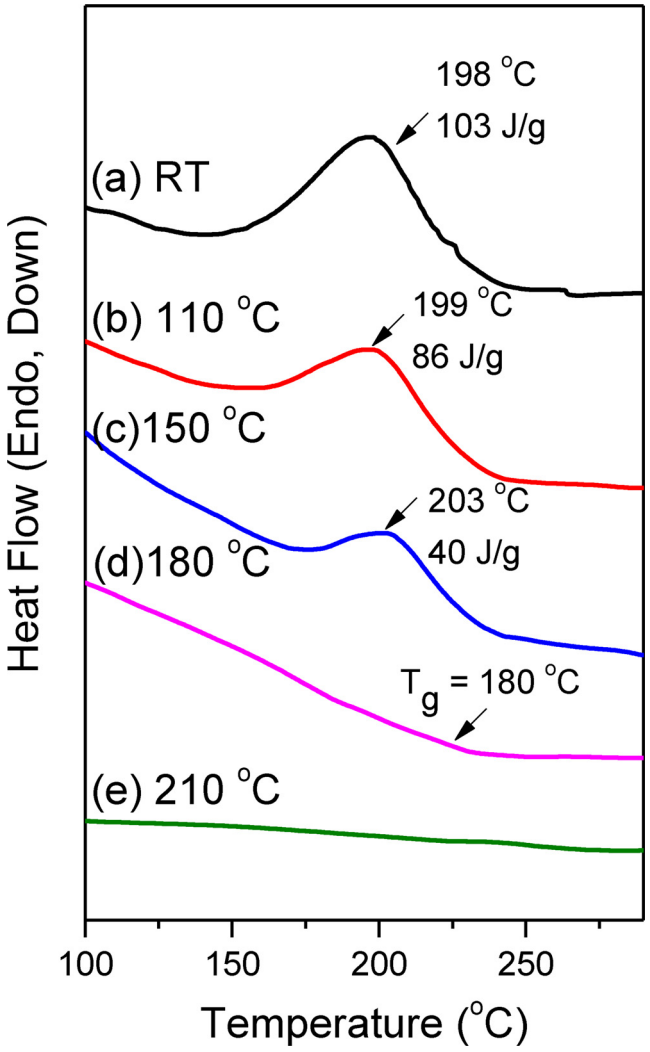

Fig. 6. DSC thermograms of CH-BZ before and after thermal treatment at various temperatures.

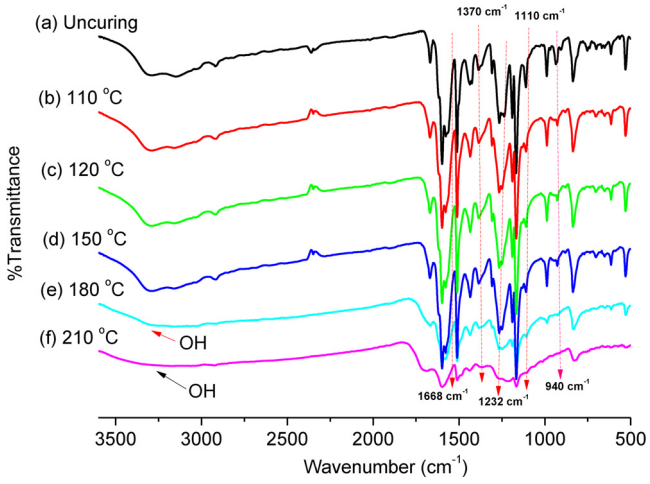

Fig. 7. FTIR spectra of CP-BZ before and after thermal treatment at various temperatures.

current density (I_{corr}), which was determined by superimposing a straight line along the linear portion of the cathodic or anodic curve and then extrapolating it through E_{corr}. The CR and the percentage protection efficiency (IE%) of each test sample were calculated using

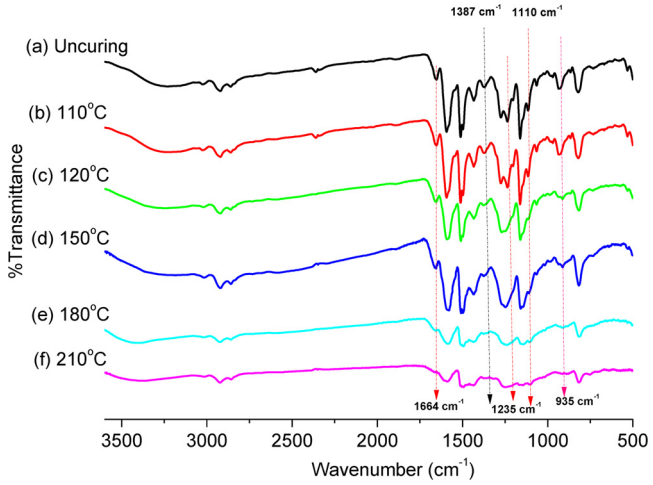

Fig. 8. FTIR spectra of CH-BZ before and after thermal treatment at various temperatures.

Eqs. (1) and (2), respectively [40,54].

$$CR = (I_{corr} \times K \times EW)/(\rho A) \quad (1)$$

where CR is the corrosion rate (mm year^{-1}), I_{corr} is the corrosion current density (A cm^{-2}), EW is the equivalent weight of the MS (g eq^{-1}), A is the area (cm^2), ρ is the density (g cm^{-3}), and K is the CR constant (3272 mm year^{-1}).

$$IE\% = [I_{corr} - I_{corr}(c)]/I_{corr} \times 100 \quad (2)$$

where I_{corr} is the corrosion current obtained for the MS and $I_{corr}(c)$ is the corrosion current for the coated MS. Each test was repeated three times at the same conditions, the average and standard deviation for E_{corr}, I_{corr}, CR and IE% values were calculated.

3. Results and discussion

3.1. Synthesis of CP-BZ and CH-BZ monomers

We synthesized the bifunctional BZ monomers containing bisbenzylidene moieties (CP-BZ and CH-BZ) through one-pot Mannich condensations of bis(benzylidene)CP-2OH and bis(benzylidene)CH-2OH, respectively, with *p*-toluidine and $(CH_2O)_n$ in 1,4-dioxane, without using any catalyst (Scheme 1). The ^{1}H NMR spectrum of CP-BZ [Fig. 1(a)] features signals at 5.30, 4.50, 2.50, 2.10, and 6.8–7.6 ppm for the OCH_2N, $ArCH_2N$, CH_2 (of CP moiety), CH_3, and aromatic protons, respectively. The ^{13}C NMR spectrum of CP-BZ [Fig. 1(b)] features signals for the carbon nuclei of the oxazine ring at 49.98 and 80.62 ppm for $ArCH_2N$ and OCH_2N, respectively.

The ^{1}H NMR spectrum of CH-BZ [Fig. 2(a)] features signals centered at 4.6 and 5.4 ppm for its $ArCH_2N$ and OCH_2N units and in the range 6.8–7.6 ppm for the protons of the aromatic and olefinic units. The ^{13}C NMR spectrum of CH-BZ [Fig. 2(b)] features signals for the carbon nuclei of the C = O group in the CH unit and the OCH_2N and $ArCH_2N$ units at 190.32, 80.38, and 50.79 ppm, respectively. We confirmed the chemical structures of the synthesized monomers from their FTIR spectra.

Figs. 3(a) and 4 (a) displays the FTIR spectra of bis(benzylidene)CP-2OH and bis(benzylidene)CH-2OH, respectively. Both spectra feature signals at 3262 cm^{-1} for the phenolic OH group, 1679 cm^{-1} for stretching of the C=O group, and 1599 cm^{-1} for stretching of the C=C bond. The FTIR spectrum of CP-BZ [Fig. 3(b)] features signals at 2917 and 2857 cm^{-1} for CH– stretching of the CP unit, 1668 cm^{-1} for the C=O group, 1467 cm^{-1} for the trisubstituted benzene ring, 1232 cm^{-1} for asymmetric stretching of the C–OC– unit, and 940 cm^{-1} for the oxazine

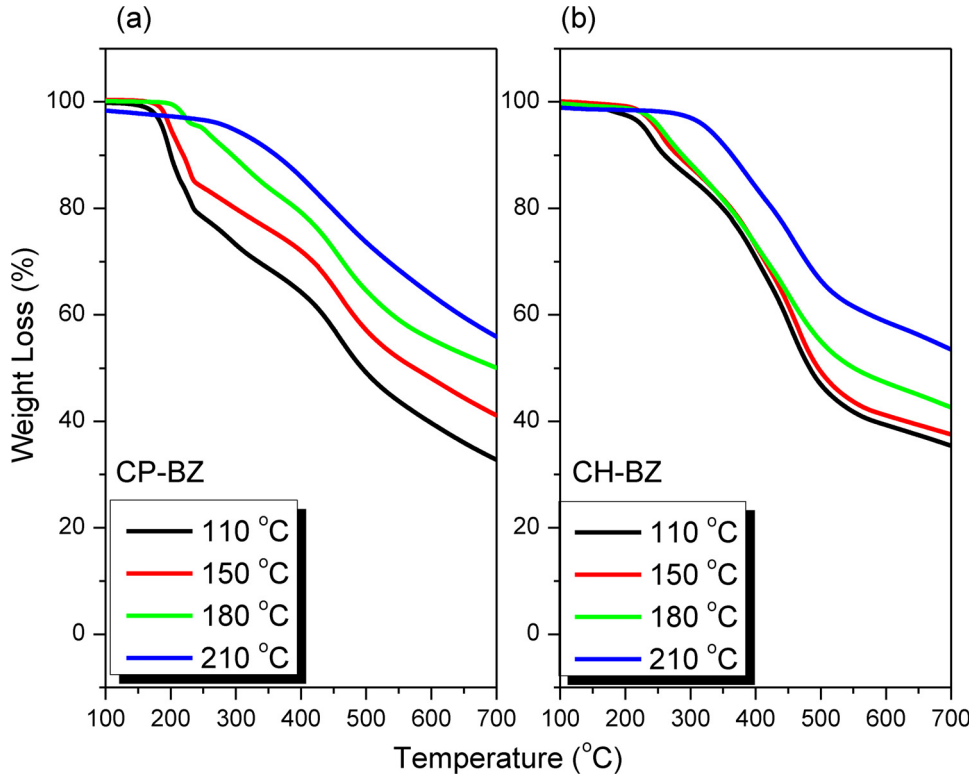

Fig. 9. TGA of (a) CP-BZ and (b) CH-BZ before and after thermal treatment at 25, 150, 180, and 210 °C.

Table 1
TGA data of CP-BZ at various thermal treatments.

Sample	T_{d5} (°C)	T_{d10} (°C)	Char yield at 800 °C
110 °C	188	200	27
150 °C	200	219	36
180 °C	249	294	46
210 °C	294	362	50

Table 2
TGA data of CH-BZ at various thermal treatments.

Sample	T_{d5} (°C)	T_{d10} (°C)	Char yield at 800 °C
110 °C	230	260	32
150 °C	249	280	34
180 °C	254	288	39
210 °C	326	364	49

ring.

The FTIR spectrum of CH-BZ [Fig. 4(b)] features signals at 1654, 1497, 1235, and 935 cm^{-1} for the C═O group, trisubstituted benzene ring, asymmetric C—OC— stretching, and the oxazine ring, respectively. After thermal ROP of CP-BZ and CH-BZ at 210 °C for 2 h, all of the characteristic bands for the oxazine rings of both BZ monomers disappeared, consistent with the formation of poly(CP-BZ) and (CH-BZ) through complete ROP.

UV spectroscopy confirmed the presence of bisbenzylidene units in the monomers CP-BZ and CH-BZ in $CHCl_3$ after irradiation at 365 nm [Figs. S4(a) and S4(b)]. Each UV absorption spectrum featured the absorption maximum near 365 nm, representing the π→π* transition of the olefinic bond in the monomer chain; the intensity of this peak decreased upon increasing the irradiation time. The photodimerization rate of the C═C bonds in CP-BZ through [2π + 2π] cycloaddition was faster than that in CH-BZ, presumably because of greater steric hindrance in CH-BZ [34].

3.2. Polymerization of CP-BZ and CH-BZ monomers

We used DSC to study the thermal polymerizations of CP-BZ and CH-BZ (Scheme 2). Figs. 5 and 6 present DSC thermograms of CP-BZ and CH-BZ, respectively, before and after thermal treatment at various temperatures. The maximum of the polymerization peak and the heat of polymerization of the uncured CP-BZ were 225 °C and 209 J g^{-1}, respectively. The maximum of the polymerization peak shifted to 198 °C for CH-BZ, with the heat polymerization decreasing to 103 J g^{-1}, due to the endotherm of melting partially overlapping with the polymerization exotherm [55]. The intensity of the polymerization exothermic peak gradually increased, while the heat of polymerization decreased, after treatment at each temperature at 110, 150, and 180 °C. At 210 °C, the ROP of the oxazine units in CP-BZ and CH-BZ was complete, forming poly(CP-BZ) and poly(CH-BZ). Interestingly, the polymerization exotherm temperatures of CP-BZ and CH-BZ were lower than that of the conventional monomer 3-phenyl-3,4-dihydro-2*H*-benzoxazine (Pa-type) (263 °C), presumably because of the presence of the olefinic bond in the main chain. Lower thermal curing temperatures for BZ monomers are highly desirable for industrial applications [56].

We also used FTIR spectroscopy to study the thermal polymerization of CP-BZ and CH-BZ (Figs. 7 and 8). The intensities of the absorption bands at 940 and 935 cm^{-1} (representing CH— out-of-plane vibrations of the benzene ring), 1110 and 1110 cm^{-1} (representing symmetric C—OC— stretching), and 1232 and 1235 cm^{-1} (representing asymmetric C—OC— stretching) for CP-BZ and CH-BZ, respectively, gradually disappeared after each thermal treatment from RT to 210 °C. The complete ROP of CP-BZ occurred after thermal curing at 210 °C, while that for CH-BZ occurred at a lower curing temperature of 180 °C, due to the latter having a lower heat of polymerization and a lower polymerization exotherm. In contrast, a broad band representing OH groups gradually increased in intensity near 3400 cm^{-1} upon increasing the curing

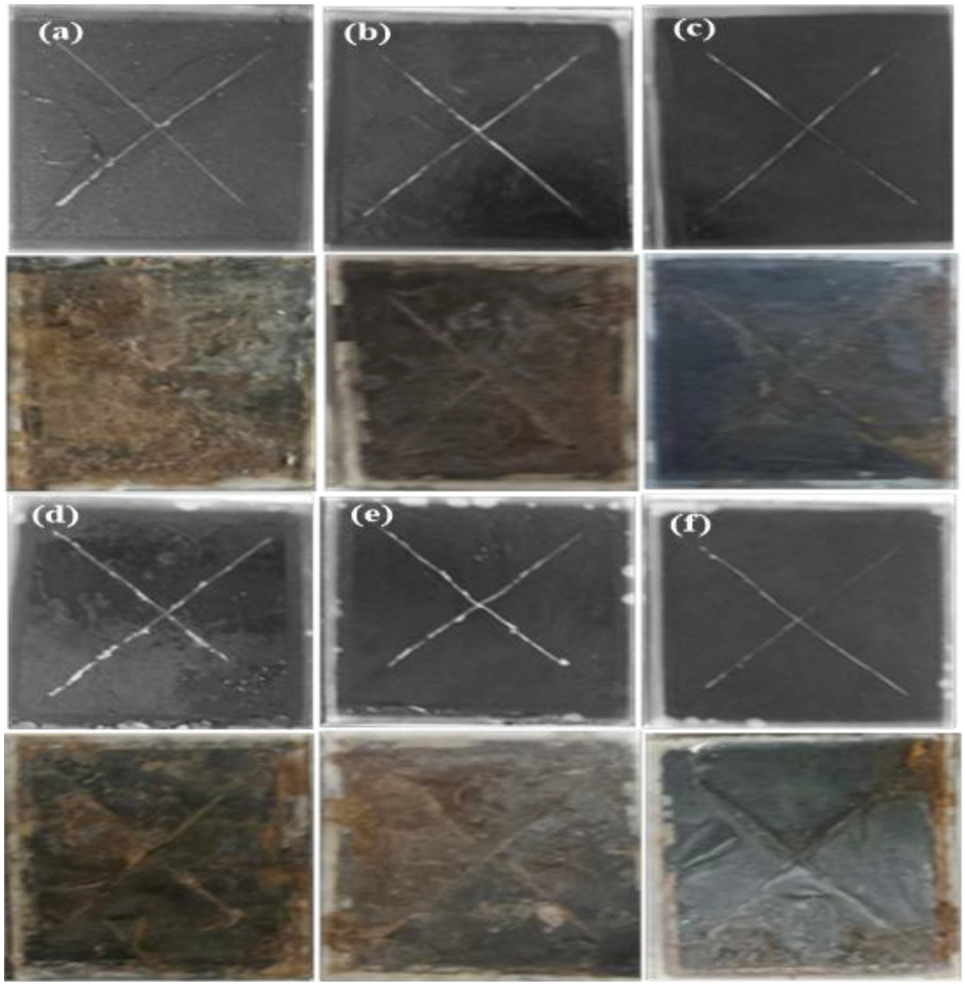

Fig. 10. MS surfaces coated with (a) pure poly(CP-BZ), (b) poly(CP-BZ)/E-SBO (10 wt%), (c) poly(CP-BZ)/E-SBO (20 wt%), (d) pure poly(CH-BZ), (e) poly(CH-BZ)/E-SBO (10 wt%), and (f) poly(CH-BZ)/E-SBO (20 wt%) for salt-spray test before and after immersed for 500 h in 5% NaCl aqueous solution.

temperature, reflecting the ring opening of the BZ units. These findings are consistent with those from the DSC analyses, confirming that the oxazine rings in CP-BZ and CH-BZ could be opened thermally, without the use of catalysts, to form highly crosslinked poly(CP-BZ) and poly (CH-BZ), respectively.

3.3. Thermal properties of uncured CP-BZ and CH-BZ before and after thermal treatment

We examined the thermal properties of the uncured CP-BZ and CH-BZ, and after their curing at 150, 180, and 210 °C, through TGA under a N_2 atmosphere at a heating rate of 20 °C min^{-1} [Fig. 9(a) and (b)]; Tables 1 and 2 summarize the results. In general, PBZs formed from bifunctional BZs feature higher degrees of crosslinking when compared with those from monofunctional BZs. We used the 5% weight loss temperature (T_{d5}), the 10 % weight loss temperature (T_{d10}), and the char yield at 800 °C to characterize the thermal stabilities of the uncured samples and those cured at 150, 180, and 210 °C. The values of T_{d5} and T_{d10} and the char yields increased significantly upon increasing the curing temperature from RT to 210 °C, due to an increase in the degree of crosslinking after each thermal curing step. Poly(CH-BZ) after curing at 210 °C exhibited a value of T_{d5} of 326 °C; this value is higher than that reported for the P-$PBZH_4$:BZH monomer UV-irradiated for 120 min followed by thermal curing (280 °C) [36]. Furthermore, poly (CP-BZ) and poly(CH-BZ) after thermal curing at 210 °C had char yields (50 and 49 %, respectively) higher than that of the conventional monomer 3-phenyl-3,4-dihydro-2*H*-benzoxazine (Pa-type) (48 %) [46,57].

3.4. Crosslinking between CP-BZ and E-SBO to form poly(CP-BZ)/E-SBO resin

FTIR spectra confirmed the existence of crosslinking between the phenolic OH groups of PBZ and the epoxide groups in the epoxy resin under thermal treatment. Fig. S5 presents the FTIR spectra of CP-BZ/E-SBO before and after curing at 210 °C for 2 h. The intensities of the absorption bands at 934 and 1320 cm^{-1} of CP-BZ/E-SBO blend before curing were significant, representing out-of-plane CH— bending vibrations of the oxazine ring of CP-BZ and the oxirane rings of the epoxy resin, respectively. After curing at 210 °C, these absorption bands disappeared and a new broad band appeared near 3432 cm^{-1}, presumably representing the stretching vibrations of self-associated OH groups in the epoxy and indicating the formation of an PBZ-epoxy network through hydroxyl–oxazine etherification [58].

3.5. Salt-spray test

Typically, salt-spray testing is used to rapidly compare expected and actual degrees of corrosion-resistance. Table S1 summarizes the degrees of blistering and scribe failure and the percentages of the areas rusted for our tested coated samples, determined after visual comparison with photographic reference standards [Fig. 10].

Pure poly(CP-BZ) and pure poly(CH-BZ) exhibited dense blistering, and their percentages of the areas rusted were greater in comparison

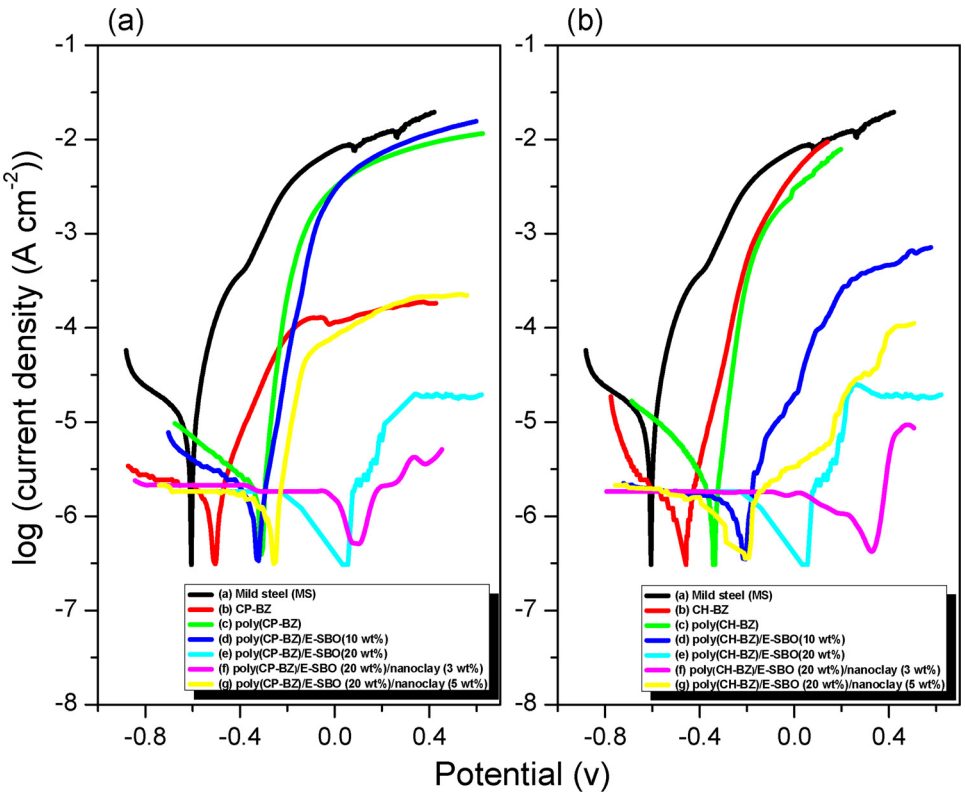

Fig. 11. (A) Tafel curves of (a) MS, (b) CP-BZ, (c) poly(CP-BZ), (d) poly(CP-BZ)/E-SBO (10 wt %), (e) poly(CP-BZ)/E-SBO (20 wt%), (f) poly (CP-BZ)/E-SBO/nanoclay (3 wt%), and (g) poly (CP-BZ)/E-SBO/nanoclay (5 wt%). (B) Tafel curves of (a) MS, (b) CH-BZ, (c) poly(CH-BZ), (d) poly(CH-BZ)/E-SBO (10 wt%), (e) poly(CH-BZ)/E-SBO (20 wt%), (f) poly(CH-BZ)/E-SBO/ nanoclay (3 wt%), and (g) poly(CH-BZ)/E-SBO/nanoclay (5 wt%) in 3.5 % NaCl aqueous solutions.

Table 3
Parameters obtained from Tafel plots for bare MS and MS samples coated with CP-BZ monomer and poly(CP-BZ) with epoxy and nanoclay at various weight percentages in 3.5 % NaCl aqueous solutions.

Sample	Corrosion Potential E_{corr} (V)	Corrosion current density, I_{corr} (A cm^{-2})	Corrosion rate, CR (mm/year)	Protection efficiency IE (%)
Blank	−0.607 ± 0.003	1.47 ± 0.009 × 10^{-5}	1.10 ± 0.010 × 10^{-1}	–
CP-BZ	−0.511 ± 0.003	2.25 ± 0.024 × 10^{-6}	1.67 ± 0.016 × 10^{-2}	85.10 ± 0.9
poly(CP-BZ)	−0.309 ± 0.004	2.32 ± 0.036 × 10^{-6}	1.72 ± 0.029 × 10^{-2}	85.4 ± 1.4
poly(CP-BZ)/E-SBO (10 wt%)	−0.331 ± 0.006	2.09 ± 0.043 × 10^{-6}	1.55 ± 0.034 × 10^{-2}	86.77 ± 1.8
poly(CP-BZ)/E-SBO (20 wt%)	0.051 ± 0.001	1.7 ± 0.045 × 10^{-6}	1.31 ± 0.034 × 10^{-2}	88.60 ± 1.5
poly(CP-BZ)/E-SBO (20 wt%)/nanoclay (3 wt%)	0.103 ± 0.003	1.12 ± 0.033 × 10^{-6}	8.21 ± 0.251 × 10^{-3}	92.81 ± 1.2
poly(CP-BZ)/E-SBO (20 wt%)/nanoclay (5 wt%)	−0.255 ± 0.009	2.0 ± 0.072 × 10^{-6}	5.53 ± 0.199 × 10^{-3}	87.14 ± 1.9

Table 4
Parameters obtained from Tafel plots for bare MS and MS samples coated with CH-BZ monomer and poly(CH-BZ) with epoxy and nanoclay at various weight percentages in 3.5 % NaCl aqueous solution.

Sample	Corrosion Potential E_{corr} (V)	Corrosion current density, I_{corr} (A cm^{-2})	Corrosion rate, CR (mm/year)	Protection efficiency IE (%)
Blank	−0.607 ± 0.003	1.46 ± 0.009 × 10^{-5}	1.10 ± 0.010 × 10^{-1}	–
CH-BZ	−0.462 ± 0.005	1.94 ± 0.034 × 10^{-6}	8.55 ± 0.097 × 10^{-3}	87.10 ± 0.9
poly(CH-BZ)	−0.340 ± 0.005	1.28 ± 0.036 × 10^{-6}	1.30 ± 0.021 × 10^{-2}	88.86 ± 1.4
poly(CH-BZ)/E-SBO (10 wt%)	−0.213 ± 0.004	1.25 ± 0.043 × 10^{-6}	7.36 ± 0.144 × 10^{-3}	92.48 ± 1.9
poly(CH-BZ)/E-SBO (20 wt%)	0.029 ± 0.0008	6.00 ± 0.045 × 10^{-7}	6.90 ± 0.175 × 10^{-3}	96.63 ± 1.6
poly(CH-BZ)/E-SBO (20 wt%)/nanoclay (3 wt%)	0.360 ± 0.010	3.22 ± 0.033 × 10^{-7}	2.70 ± 0.079 × 10^{-3}	98.16 ± 1.2
poly(CH-BZ)/E-SBO (20 wt%)/nanoclay (5 wt%)	−0.230 ± 0.008	2.17 ± 0.072 × 10^{-6}	8.69 ± 0.301 × 10^{-3}	93.94 ± 2.0

with the other coatings containing E-SBO resin. Thus, these coatings underwent drastic chemical changes during exposure, leading to failure. In contrast, the MS samples coated with poly(CP-BZ)/E-SBO (10 or 20 wt%) and poly(CH-BZ)/E-SBO (10 or 20 wt%) exhibited good adhesion, with no more dispersion of corrosion along and around the cross cut, indicating that these coatings had good corrosion-resistance. Furthermore, the corrosion-resistance increased upon increasing the content of E-SBO resin in the coatings [41], due to the formation of highly crosslinked PBZ/E-SBO epoxy resin networks during the curing process. In addition, the transport rate of water along the cross cut of the coating decreased significantly upon increasing the content of E-SBO.

3.6. Electrochemical results

We used potentiodynamic polarization to study the corrosion-resistance of bare steel (blank) and poly(CP-BZ)– and poly(CH-BZ)–coated MS plates, containing various weight percentages of the

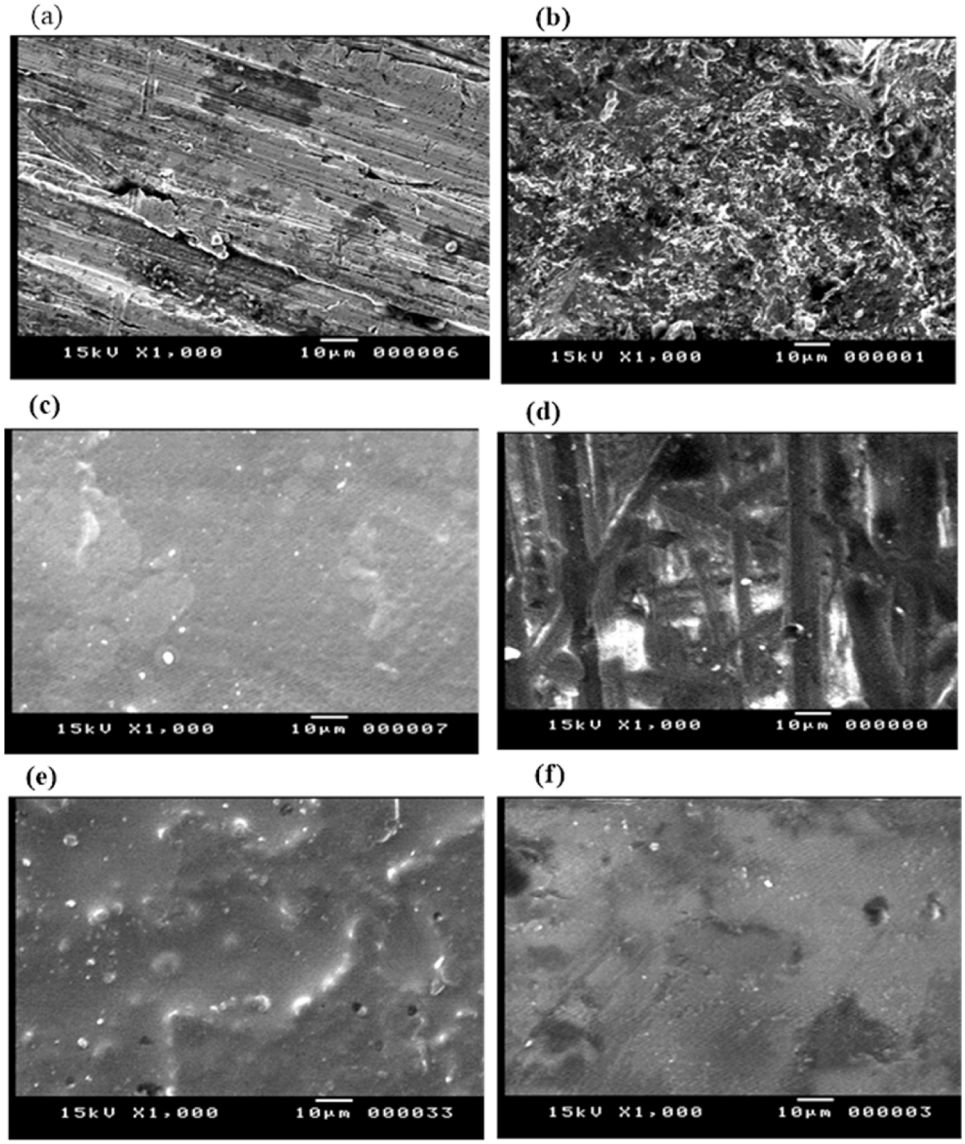

Fig. 12. SEM images of (a, b) MS in the absence of any polymer coating, (c, d) MS coated with neat poly(CH-BZ), and (e, f) MS coated with poly(CH-BZ)/E-SBO/nanoclay (3 wt%) before and after immersion in 3.5 % NaCl.

epoxy and nanoclay (Fig. S6). We tested these samples in 3.5 wt% aqueous NaCl at room temperature. Fig. 11(A) and (B) present the Tafel curves of the bare and coated steel samples.

Tables 3 and 4 summarize the values of E_{corr} and I_{corr} and the CRs and protection efficiencies. In general, a more negative value of E_{corr} and a higher value of I_{corr} indicate greater susceptibility toward corrosion, while a more positive value of E_{corr} and a lower value of I_{corr} indicate low susceptibility toward corrosion [59]. The protection efficiencies of poly(CP-BZ) and poly(CH-BZ) with E-SBO were higher than that of the neat PBZs, suggesting that presence of the epoxy resin in the polymer matrices enhanced the coating adhesion with the metal substrate. As a result, the MS samples coated with poly(CP-BZ) and poly (CH-BZ) containing E-SBO had their corrosion potentials E_{corr} shifted to more positive values, in comparison with those of the neat poly(CP-BZ) and poly(CH-BZ). The values of E_{corr} of poly(CP-BZ) and poly(CH-BZ) were –0.309 and –0.340 V, respectively; they shifted to more positive potentials for poly(CP-BZ)/E-SBO (10 wt%) (-0.331 V) and poly(CH-BZ)/E-SBO (10 wt%) (–0.213 V). These shifts in the values of E_{corr} in the positive direction indicate passivation effects for these coatings [60]. We suspect that the presence of high-density crosslinking and the aliphatic chains of the epoxy resin in the coatings markedly improved the barrier properties of these coatings toward corrosive species. Meanwhile, phenolic OH groups in the PBZs reacted with the epoxide groups to form a denser polymer network, thereby decreasing the sizes of the micropores inside the coating matrices as the percentage content of the epoxy increased. Furthermore, the corrosion potential of poly(CH-BZ)/E-SBO (20 wt%) (0.029 V) much higher positively than that reported previously for PBE40-coated MS at a concentration of 180 mg mL^{-1} (–0.45 V) with a 40 % epoxy content [41]. The CRs of the poly(CH-BZ)/E-SBO/nanoclay (3 wt%) composites were 2.653×10^{-3} mm $year^{-1}$, respectively; these values are much lower than those reported previously for a poly(Azine-BZ-CH_3)/nanoclay(3)/E-SBO coating (9 mm $year^{-1}$) [46] and for a bisphenol A–based PBZ (PBA-a) coating at a concentration of 100 g L^{-1} (5.75×10^{-3} mm $year^{-1}$) [61]. Similarly, the corrosion current of the bare steel sample (1.47×10^{-5} A cm^{-2}) was much higher than those for the poly(CH-BZ)/E-SBO/nanoclay (3 wt%) (3.22×10^{-7}A cm^{-2}) and poly(CP-BZ/E-SBO/nanoclay (3 wt%) (1.12×10^{-6} A cm^{-2}) composites. The MS coated with poly(CH-BZ)/E-SBO) in the presence of 3 wt% nanoclay provided the highest corrosion protection performance (98.16 %), when compared with the other MS coated. Also, It was observed that the MS coated with poly(CH-BZ) showed higher corrosion resistance performance than that of MS coated

with poly(CP-BZ) due to the poly(CH-BZ) providing higher covering in the system. The positive shift in the values of E_{corr} for the poly(CP-BZ)/E-SBO/nanoclay (3 wt%) composite coatings which are indicates that the incorporation of nanoparticles (NPs) suppressed anodic reactions on the steel surface and, thereby, inhibited the entire corrosion process in the system [62]. In addition, the presence of 5 wt% nanoclay in the PBZ/epoxy matrices caused negative effects, due to decreases in the degrees of intercalation of the nanoclay and increases in the saturation levels of the nanoclay into the PBZ/epoxy matrices, consequently generating areas of agglomeration that could be identified as weaknesses in the polymer coatings [63].

3.7. Surface morphologies

The functionalization of NPs is necessary to achieve their greatest dispersion within PBZ matrices by maximizing interfacial adhesion between the polymeric matrix and the NPs [64]. We used SEM to investigate the surface properties of the bare MS and the MS coated with the neat poly(CH-BZ) and poly(CH-BZ)/E-SBO/nanoclay (3 wt%) composites before and after the immersion in 3.5 wt% NaCl aqueous solution (Fig. 12). The SEM image of the MS in the absence of any coating revealed a very rough surface with pits and cracks [Fig. 12(a)]. In contrast, the MS samples had smooth surfaces after their coating with the neat poly(CH-BZ) and poly(CH-BZ)/E-SBO/nanoclay (3 wt%) composites. The roughness of the surfaces increased when the PBZ matrices were reinforced with the various weight percentages of the epoxy and nanoclay, as shown in [Fig. 12(c) and (e)]. The surface of the MS in the absence of any coating completely damaged after exposure to the 3.5 wt % NaCl aqueous solution for 30 min [Fig. 12(b)]. As presented in Figures (d) and (f), the pits and cracks of the MS coated decreased after MS coated with neat poly(CH-BZ) poly(CH-BZ)/E-SBO/nanoclay (3 wt%). These results indicate that MS displayed high corrosion resistance performance in presence of the 20 wt % of E-SBO and 3 wt % of nanoclay.

Fig. S7 presents TEM images of the poly(CH-BZ)/E-SBO/nanoclay (3 wt%) hybrid composites at different degrees of magnification. As seen in Fig. S7, the presence dark lines and bright regions in these images, revealing partially exfoliated/intercalated structures for this coating [65]. The individual silicate layers are dispersed in PBZ/E-SBO matrix. However, the complete of exfoliation and intercalation are not achieved due to aggregates of silicate layers [66]. The improvement of corrosion resistance of PBZ/E-SBO/clay nanocomposite coatings may be attributed to the well dispersed of clay nanolayers through PBZ/E-SBO network matrix which caused in the increase the barrier properties of coating and decrease the penetration of water and corrosive ions.

4. Conclusions

We have synthesized the bifunctional BZ monomers CP-BZ and CH-BZ containing bisbenzylidene moieties and confirmed their structures using ^{1}H and ^{13}C NMR and FTIR spectroscopy. We used DSC and FTIR spectroscopy to study the curing behavior of these monomers. The temperature for ring opening of CH-BZ (198 °C) was lower than that of CP-BZ (225 °C), suggesting a steric effect. According to TGA, the values of T_{d5} and T_{d10} and the char yields increased significantly upon increasing the curing temperature from RT to 210 °C, due to an increase in the degree of crosslinking after each thermal curing step. We used salt-spray and polarization measurements to examine the degrees of corrosion of coated MS. The presence of E-SBO and nanoclay in the PBZ composites provided coatings exhibiting excellent adhesion to the MS surface and high interfacial strength, respectively, leading to these sample exhibiting the highest corrosion-resistance after exposure to NaCl solution. The barrier properties of the coatings improved by decreasing their permeability and increasing the length of the diffusion pathways for O_2 and water. SEM and TEM confirmed that the clay NPs were dispersed within the coating matrices. The PBZ/E-SBO/nanoclay (3 wt%) composite appears to be suitable for use as an MS surface coating for high-performance anticorrosive coating applications.

CRediT authorship contribution statement

Mohamed Gamal Mohamed: Supervision, Investigation, Formal analysis, Writing - original draft, Writing - review & editing. **Shiao Wei Kuo:** Supervision. **Abdulsalam Mahdy:** Investigation. **Ibrahim M. Ghayd:** Supervision. **Kamal. I. Aly:** Supervision, Writing - original draft, Writing - review & editing.

Declaration of Competing Interest

The authors declare that they have no conflicts of interest.

Acknowledgments

The authors acknowledge financial support from the Science and Technology Development Fund (STDF, Egypt) (call 6/STDF Basic and Applied Research Grants (STDF-BARG)/Basic and Applied Research Grants) Project ID: 28930.

Appendix A. Supplementary data

Supplementary material related to this article can be found, in the online version, at doi:https://doi.org/10.1016/j.mtcomm.2020.101418.

References

[1] K. Zhang, Y. Liu, H. Ishida, Polymerization of an AB-type benzoxazine monomer toward different polybenzoxazine networks: when Diels–Alder reaction meets benzoxazine chemistry in a single-component resin, Macromolecules 52 (2019) 7386–7395, https://doi.org/10.1021/acs.macromol 9b01581.
[2] F.S. Gungor, B. Bati, B. Kiskan, Combining naphthoxazines and benzoxazines for non-symmetric curable oxazines by one-pot synthesis, Eur. Polym. J. 121 (2019) 109352–109358, https://doi.org/10.1016/j.eurpolymj.2019.109352.
[3] M.G. Mohamed, S.W. Kuo, Crown ether-functionalized polybenzoxazine for metal ion adsorption, Macromolecules 53 (2020) 2420–2429, https://doi.org/10.1021/acs.macromol.9b02519.
[4] H.K. Shih, C.C. Hsieh, M.G. Mohamed, C.Y. Zhu, S.W. Kuo, Ternary polybenzoxazine/POSS/ SWCNT hybrid nanocomposites stabilized through supramolecular interactions, Soft Matter 12 (2016) 1847–1858, https://doi.org/10.1039/C5SM02569A.
[5] K. Zhang, X.X. Tan, Y.T. Wang, H. Ishida, Unique self-catalyzed cationic ring-opening polymerization of a high performance deoxybenzoin-based 1,3-benzoxazine monomer, Polymer 168 (2019) 8–15, https://doi.org/10.1016/j.polymer.2019.01.089.
[6] M.G. Mohamed, S.W. Kuo, Functional silica and carbon nanocomposites based on polybenzoxazines, Macromol. Chem. Phys. 220 (2019) 1800306–1800318, https://doi.org/10.1002/macp.201800306.
[7] M.G. Mohamed, K.C. Hsu, S.W. Kuo, Bifunctional polybenzoxazine nanocomposites containing photo-crosslinkable coumarin units and pyrene units capable of dispersing single-walled carbon nanotubes, Polym. Chem. 6 (2015) 2423–2433, https://doi.org/10.1039/C5PY00035A.
[8] R.C. Lin, M.G. Mohamed, K.C. Hsu, J.Y. Wu, Y.R. Jheng, S.W. Kuo, Multivalent photo-crosslinkable coumarin-containing polybenzoxazines exhibiting enhanced thermal and hydrophobic surface properties, RSC Adv. 6 (2016) 10683–10696, https://doi.org/10.1039/C5RA27705A.
[9] K. Zhang, X. Yu, S.W. Kuo, Outstanding dielectric and thermal properties of main chain-type poly(benzoxazine-co-imide-co-siloxane)-based cross-linked networks, Polym. Chem. 10 (2019) 2387–2396, https://doi.org/10.1039/C9PY00464E.
[10] B. Kiskan, Adapting benzoxazine chemistry for unconventional applications, React. Funct. Polym. 129 (2018) 76–88, https://doi.org/10.1016/j.reactfunctpolym.2017.06.009.
[11] W. Shi, X. Zhang, Y. Ji, Z. Zhao, W. Li, X. Jia, Sustainable preparation of bio-based polybenzoxazine resins from amino acid and their application in CO_2 adsorption, ACS Sustain. Chem. Eng. 7 (2019) 17313–17324, https://doi.org/10.1021/acssuschemeng.9b04163.
[12] R.C. Lin, M.G. Mohamed, S.W. Kuo, Benzoxazine/triphenylamine-based dendrimers prepared through facile one-pot mannich condensations, Macromol. Rapid Commun. 38 (2017) 1700251–1700257, https://doi.org/10.1002/marc.201700251.
[13] Y. Wang, K. Kou, Z. Li, G. Wu, Y. Zhang, A. Feng, Synthesis, characterization, and thermal properties of benzoxazine monomers containing allyl groups, High Perform. Polym. 28 (2016) 1235–1245, https://doi.org/10.1039/C9RA10191H.

[14] P. Froimowicz, C.R. Arza, C.L. Han, H. Ishida, Smart, sustainable, and ecofriendly chemical design of fully bio-based thermally stable thermosets based on benzoxazine chemistry, ChemSusChem 9 (2016) 1921–1928, https://doi.org/10.1002/cssc.201600577.
[15] M.G. Mohamed, W.C. Su, Y.C. Lin, C.F. Wang, J.K. Chen, K.U. Jeong, S.W. Kuo, Azopyridine-functionalized benzoxazine with $Zn(ClO4)_2$ form high-performance polybenzoxazine stabilized through metal–ligand coordination, RSC Adv. 4 (2014) 50373–50385, https://doi.org/10.1039/C4RA08381D.
[16] S. Sarojadevi, Synthesis, characterization, curing, and thermal properties of bi-functional phenol-based polybenzoxazines, High Perform. Polym. 28 (2015) 331–339, https://doi.org/10.1177/0954008315580822.
[17] X. Zhang, M.G. Mohamed, Z. Xin, S.W. Kuo, A tetraphenylethylene-functionalized benzoxazine and copper (II) acetylacetonate form a high-performance polybenzoxazine, Polymer 201 (2020) 122552, , https://doi.org/10.1016/j.polymer.2020.122552 201.
[18] S. Shukla, B. Lochab, Role of higher aromatic content in modulating properties of cardanol based benzoxazines, Polymer 99 (2016) 684–694, https://doi.org/10.1016/j.polymer.2016.07.074.
[19] J.Y. Wu, M.G. Mohamed, S.W. Kuo, Directly synthesized nitrogen-doped microporous carbons from polybenzoxazine resins for carbon dioxide capture, Polym. Chem. 8 (2017) 5481–5489, https://doi.org/10.1039/C7PY01026E.
[20] M.G. Mohamed, S.W. Kuo, Polybenzoxazine/polyhedral oligomeric silsesquioxane (POSS) nanocomposites, Polymers 8 (2016) 225–234, https://doi.org/10.3390/polym8060225.
[21] W.C. Chen, S.W. Kuo, Ortho-imide and allyl groups effect on highly thermally stable polybenzoxazine/double-decker-shaped polyhedral silsesquioxane hybrids, Macromolecules 51 (2018) 9602–9612, https://doi.org/10.1021/acs.macromol.8b02207.
[22] Y. Lyu, E. Rachita, N. Pogharian, P. Froimowicz, H. Ishida, Electronic effects of asymmetric and meta-alkoxy substituents on the polymerization behavior of bis-benzoxazines, Polym. Chem. 11 (2020) 800–809, https://doi.org/10.1039/C9PY01641D.
[23] C. Zhu, X. Gao, W. Fan, X. Fu, Synthesis, characterization, and properties of a novel aromatic ester-based polybenzoxazine, RSC Adv. 10 (2020) 6953–6959, https://doi.org/10.1039/C9RA10191H.
[24] Y. Liu, R. Yin, X. Yu, K. Zhang, Modification of solventless synthesized benzoxazine resin by phthalonitrile group: an effective approach for enhancing thermal stability of polybenzoxazines, Macromol. Chem. Phys. 220 (2018) 1800291–1800297, https://doi.org/10.1002/macp.201800291.
[25] D.M. Patil, G.A. Phalak, S.T. Mhaske, Enhancement of anti-corrosive performances of cardanol based amine functional benzoxazine resin by copolymerizing with epoxy resins, Prog. Org. Coat. 105 (2017) 18–28, https://doi.org/10.1016/j.porgcoat.2016.10.027.
[26] G.P. Cao, W.J. Chen, X.B. Liu, Synthesis and thermal properties of the thermosetting resin based on cyano functionalized benzoxazine, Polym. Degrad. Stab. 93 (2008) 739–744, https://doi.org/10.1016/j.polymdegradstab.2007.10.002.
[27] M.G. Mohamed, C.H. Hsiao, F. Luo, L. Dai, S.K. Kuo, Multifunctional polybenzoxazine nanocomposites containing photoresponsive azobenzene units, catalytic carboxylic acid groups, and pyrene units capable of dispersing carbon nanotubes, RSC Adv. 5 (2015) 45201–45212, https://doi.org/10.1039/C5RA07983G.
[28] R.C.S. Pereira, L.R.V. Kotzebue, D. Zampieri, G. Mele, S.E. Mazzetto, D. Lomonaco, Influence of natural substituents in the polymerization behavior of novel bio-based benzoxazines, Mater. Today Commun. 21 (2019) 100629-, https://doi.org/10.1016/j.mtcomm.2019.100629.
[29] Y. Peng, J. Dai, Y. Liu, L. Cao, J. Zhu, X. Liu, Bio-based polybenzoxazine modified melamine sponges for selective absorption of organic solvent in water, Adv. Sustainable Syst. 3 (2019) 1800126–1800135, https://doi.org/10.1002/adsu.201800126.
[30] C. Andronescu, S.A. Gârea, C. Deleanu, H. Iovu, Characterization and curing kinetics of new benzoxazine monomer based on aromatic diamines, Thermochim. Acta 530 (2012) 42–51, https://doi.org/10.1016/j.tca.2011.11.035.
[31] Y. Liu, J. Zhang, C. Liao, J. Zheng, S. Zhao, M. Run, Morphology and thermal properties of copolymer based on p-aminobenzonitrile type benzoxazine and diglycidyl ether of bisphenol-A, Thermochim. Acta 573 (2013) 138–145, https://doi.org/10.1016/j.tca.2013.09.031.
[32] M. Murali, A.B. Samui, Bisbenzylidene cycloalkanone: a versatile molecule as a polymer building block, J. Mater. Chem. 20 (2010) 2714–2737, https://doi.org/10.1039/B915137K.
[33] R. Balamurugan, P. Kannan, Photoreactive main chain liquid crystalline polyesters containing oxadiazole and bis(benzylidene) cycloalkanone units, J. Polym. Sci. Part A: Polym. Chem. 46 (2008) 5760–5775, https://doi.org/10.1002/pola.22891.
[34] C.H. Lin, Z.J. Chen, C.H. Chen, M.W. Wang, T.Y. Juang, Synthesis of a bisbenzylideneacetone-containing benzoxazine and its photo- and thermally cured thermoset, ACS Omega 2 (2017) 3432–3440, https://doi.org/10.1021/acsomega.7b00573.
[35] C.H. Lin, C.K. Chien, C.H. Chen, T.Y. Juang, Photo-sensitive benzoxazine II: chalcone-containing benzoxazine and its photo and thermal-cured thermoset, RSC Adv. 7 (2017) 37844–37851, https://doi.org/10.1039/C7RA06967G.
[36] M.R. Vengatesan, S. Devaraju, M. Selvi, A. Chandramohan, A.A. Kumar, M. Alagar, Photolysis and thermal active polymerization of bis (benzylidene) based benzoxazine monomers, J. Mol. Struct. 1027 (2012) 162–166, https://doi.org/10.1016/j.molstruc.2012.06.002.
[37] K.I. Aly, A.A. Khalaf, I.A. Mohamed, New polymer syntheses XII polyketones based on diarylidenecycloalkanones, Eur. Polym. J. 39 (2003) 1273–1279, https://doi.org/10.1016/S0014-3057(02)00365-8.
[38] N.S. Al-Muaikel, K.I. Aly, M.A. Hussien, Synthesis, characterization and antimicrobial properties of new poly (ether-ketone)s and copoly(ether-ketone)s containing diarylidenecycloalkanone moieties in the main chain, J. Appl. Polym. Sci. 108 (2008) 3138–3314, https://doi.org/10.1002/app.27963.
[39] K.I. Aly, Liquid crystalline polymers. 3. Synthesis and liquid crystal properties of thermotropic poly(arylidene-ether)s and copolymers containing cycloalkanones moiety in the polymer backbone, J. Macromol. Sci. A 37 (2000) 93–115, https://doi.org/10.1081/MA-100101083.
[40] R. Ambrožič, U. Šebenik, M. Krajnc, Epoxy emulsions stabilized with reactive bio-benzoxazine surfactant from epoxidized cardanol for coatings, Eur. Polym. J. 81 (2016) 138–151, https://doi.org/10.1016/j.eurpolymj.2016.05.029.
[41] C. Zhou, J. Lin, X. Lu, Z. Xin, Enhanced corrosion resistance of polybenzoxazine coatings by epoxy incorporation, RSC Adv. 6 (2016) 28428–28434, https://doi.org/10.1039/C6RA02215D.
[42] V. Selvaraj, T.R. Raghavarshini, M. Alagar, Development of Prosopis juliflora carbon-reinforced PET bottle waste-based epoxy-blended bio-phenolic benzoxazine composites for advanced applications, RSC Adv. 10 (2012) 5656–5665, https://doi.org/10.1039/C9RA08741A.
[43] S. Rimdusit, P. Kunopast, I. Dueramae, Thermomechanical properties of arylamine-based benzoxazine resins alloyed with epoxy resin, Polym. Eng. Sci. 51 (2011) 1797–1807, https://doi.org/10.1002/pen.21969.
[44] G.A. Phalak, D.M. Patil, S.T. Mhaske, Synthesis and characterization of thermally curable guaiacol based poly(benzoxazine-urethane) coating for corrosion protection on mild steel, Eur. Polym. J. 88 (2017) 93–108, https://doi.org/10.1016/j.eurpolymj.2016.12.030.
[45] T. Takeichi, R. Zeidam, T. Agag, Polybenzoxazine/clay hybrid nanocomposites: influence of preparation method on the curing behavior and properties of polybenzoxazines, Polymer 43 (2002) 45–53, https://doi.org/10.1016/S0032-3861(01)00604-8.
[46] K.I. Aly, M.G. Mohamed, O. Younis, M.H. Mahross, M.A. Hakim, M.M. Sayed, Salicylaldehyde azine-functionalized polybenzoxazine: synthesis, characterization, and its nanocomposites as coatings for inhibiting the mild steel corrosion, Prog, Org. Coat. 138 (2020) 105385, https://doi.org/10.1016/j.porgcoat.2019.105385.
[47] A. Hariharan, P. Prabu Nathan, A. Kumaravel, M. Manoj, M. Alagar, Bio-based polybenzoxazine composites for oil-water separation, sound absorption and corrosion resistance applications, Polym. Test. 86 (2020) 106443, https://doi.org/10.1016/j.polymertesting.2020.106443.
[48] B. Bălănucă, M. Raicopol, A. Maljusch, S. Garea, A. Hanganu, W. Schuhmann, C. Andronescu, Phenolated oleic acid based polybenzoxazine derivatives as corrosion protection layers, ChemPlusChem 80 (2015) 1170–1177, https://doi.org/10.1002/cplu.201500092.
[49] D.M. Patil, G.A. Phalak, S.T. Mhaske, Synthesis, and characterization of bio-based benzoxazine oligomer from cardanol for corrosion resistance application, J. Coat. Technol. Res. 14 (2017) 517–530, https://doi.org/10.1007/s11998-016-9892-3.
[50] M. Raicopol, B. Bălănucă, K. Sliozberg, B. Schlüter, S.A. Gârea, N. Chira, W. Schuhmann, C. Andronescu, Vegetable oil-based polybenzoxazine derivatives coatings on Zn–Mg–Al alloy coated steel, Corros. Sci. 100 (2015) 386–395, https://doi.org/10.1016/j.corsci.2015.08.018.
[51] M.A. Abd-Alla, M.M. Kandeel, K.I. Aly, A.S. Hammam, Aryudene polymers. II Synthesis and characterization of some new polyesters of diarylidenecyclopentanone, J. Macromol. Sci. chem. 27 (1990) 523–538, https://doi.org/10.1080/00222339009349640.
[52] A.V. Raghu, G. Anita, Y.M. Barigaddi, G.S. Gadaginamath, T.M. Aminabhavi, Synthesis and characterization of novel polyurethanes based on 2,6-bis (4-hydroxybenzylidene) cyclohexanone hard segments, J. Appl. Polym. Sci. 104 (2007) 81–88, https://doi.org/10.1002/app.25518.
[53] A.M. El Saeed, M.A. El-Fattah, A.M. Azzam, Synthesis of ZnO nanoparticles and studying its influence on the antimicrobial, anticorrosion and mechanical behavior of polyurethane composite for surface coating, Dyes Pigm. 121 (2015) 282–289, https://doi.org/10.1016/j.dyepig.2015.05.037.
[54] K.I. Aly, M.A. Hussein, Synthesis, characterization and corrosion inhibitive properties of new thiazole based polyamides containing diarylidenecyclohexanone moiety, Chin. J. Polym. Sci. 32 (2015) 1–13, https://doi.org/10.1007/s10118-015-1569-3.
[55] K. Zhang, J. Liu, S. Ohashi, X. Liu, Z. Han, H. Ishida, Synthesis of high thermal stability polybenzoxazoles via ortho-imide-Functional benzoxazine monomers, J. Polym. Sci. Part A: Polym. Chem. 53 (2015) 1330–1338, https://doi.org/10.1002/pola.27565.
[56] M. Arslan, B. Kiskan, Y. Yagci, Ring-opening polymerization of 1,3-benzoxazines via borane catalyst, Polymers 10 (2018) 239–251, https://doi.org/10.3390/polym10030239.
[57] M.G. Mohamed, R.C. Lin, J.H. Tu, F.H. Lu, J.L. Hong, K.U. Jeong, C.F. Wang, S.W. Kuo, Thermal property of an aggregation-induced emission fluorophore that forms metal-ligand complexes with $Zn(ClO_4)_2$ of salicylaldehyde azine-functionalized polybenzoxazine, RSC Adv. 5 (2015) 65635–65645, https://doi.org/10.1039/C5RA09409G.
[58] C. Zhou, X. Lu, Z. Xin, J. Liu, Y. Zhang, Hydrophobic benzoxazine-cured epoxy coatings for corrosion protection, Prog. Org. Coat. 76 (2013) 1178–1183, https://doi.org/10.1016/j.porgcoat. 2013.03.013.
[59] Y. Zhang, X. Liu, G. Zhan, Q. Zhuang, R. Zhan, G.J. Qian, Study on the synergistic anticorrosion property of a fully bio-based polybenzoxazine copolymer resin, Eur. Polym. J. 119 (2019) 477–486, https://doi.org/10.1016/j.eurpolymj.2019.07.020.
[60] F. Zulkifli, M.S.M. Yusof, M.I.N. Isa, A. Yabuki, W.W.B. Nik, Henna leaves extract as a corrosion inhibitor in acrylic resin coating, Prog. Org. Coat. 105 (2017) 310–319, https://doi.org/10.1016/j.porgcoat.2017.01.017.
[61] X. Lu, Y. Liu, C. Zhou, W. Zhang, Z. Xin, Corrosion protection of hydrophobic bisphenol A-based polybenzoxazine coatings on mild steel, RSC Adv. 6 (2016) 5805–5811, https://doi.org/10.1039/C5RA22980D.

[62] C. Zhou, X. Lu, Z. Xin, J. Liu, Y. Zhang, Polybenzoxazine/SiO_2 nanocomposite coatings for corrosion protection of mild steel, Corros. Sci. 80 (2014) 269–275, https://doi.org/10.1016/j.corsci.2013.11.042.
[63] E.H. Saarivirta, G.V. Vaganov, V.E. Yudin, J. Vuorinen, Characterization and corrosion protection properties of epoxy powder coatings containing nanoclays, Prog. Org. Coat. 76 (2013) 757–767, https://doi.org/10.1016/j.porgcoat.2013.01.005.
[64] Q. Xu, M. Zeng, Z. Feng, D. Yin, Y. Huang, Y. Chen, C. Yan, R. Lia, Y. Gu, Understanding the effects of carboxylated groups of functionalized graphene oxide on the curing behavior and intermolecular interactions of benzoxazine nanocomposites, RSC Adv. 6 (2016) 31484–31496, https://doi.org/10.1039/C5RA28016H.
[65] F.T. Shirehjini, I. Danaee, H. Eskandari, D. Zarei, Effect of nano clay on corrosion protection of Zinc-rich epoxy coatings on steel 37, J. Mater. Sci. Technol. 32 (2016) 1152–1160, https://doi.org/10.1016/j.jmst.2016.08.017.
[66] A. Das, D. Wang, K.W. Stockelhuber, R. Jurk, J. Fritzsche, M. Klueppel, G. Heinrich, Rubber–clay nanocomposites: some recent results, Adv. Polym. Sci. 239 (2011) 85–166, https://doi.org/10.1007/12_2010_96.